AIMS Mathematics, 10(1): 654–671.
DOI: 10.3934/math.2025029
Received: 23 October 2024
Revised: 18 December 2024
Accepted: 26 December 2024
Published: 13 January 2025

https://www.aimspress.com/journal/Math

Research article

Improved region-based active contour segmentation through divergence and convolution techniques

Ming Shi[1,*] **and Ibrar Hussain**[2]

[1] Department of Computer and Information Engineering, Shanxi Institute of Energy, Taiyuan 030000, China

[2] Department of Mathematics, University of Peshawar, Peshawar 25120, Pakistan

* **Correspondence:** Email: shiming171012@outlook.com.

Abstract: In this paper, we present a novel approach to improve the robustness of region-based active contour models for image segmentation, particularly in the presence of noise. Traditional active contour methods often struggle with noise sensitivity and intensity variations within the image. To overcome these limitations, we propose an enhanced segmentation model that integrates the average convolution with entropy-based mean gray level values. Our method leverages the local statistical information by introducing a local similarity factor and local region relative entropy to build a robust energy functional. This energy functional balances the intensity differences between neighboring pixels and regions within the local window, while reducing the impact of noise. By incorporating convolution and entropy into the energy formulation, our model distinguishes between the interior and exterior regions of an image more effectively, thus leading to more accurate segmentation results. We demonstrate the numerical implementation of the proposed model, along with its convexity properties, to ensure stability and reliability. The experimental results show that our method significantly improves the segmentation performance, even in challenging scenarios with varying noise levels. This advancement has the potential to improve image analyses in fields such as medical imaging, object detection, and texture classification.

Keywords: image segmentation; averaging filter; level set method; Euler Langrange equation; relative entropy; objects
Mathematics Subject Classification: 68U10, 62H35

1. Introduction

Image segmentation is a fundamental task in computer vision and applied mathematics, involving the division of an image into distinct, meaningful regions that correspond to objects or surfaces in

the scene [1–4]. Accurate segmentation is essential for various downstream tasks, such as object recognition and scene understanding. Over the years, a wide range of methods have been proposed for image partitioning, thus reflecting the importance of this task in areas such as medical imaging, remote sensing, and autonomous driving [5–8]. Among these, active contour models (ACMs) within the level-set framework have emerged as a prominent approach, thereby offering a balance between simplicity and robustness. These models can be broadly classified into two main types: edge-based segmentation models [9–13] and region-based segmentation models [14–18].

Edge-based active contours are driven by gradient information, thereby guiding the contour towards object boundaries. While effective in well-structured images, they are highly sensitive to noise and often struggle with weak or poorly defined boundaries. In contrast, region-based ACMs leverage the statistical information of regions rather than relying on gradients. This makes them more resilient in complex scenarios, where noise or weak boundaries pose significant challenges. By using information from larger regions of the image, region-based methods can often achieve more reliable and accurate segmentation, making them a preferred choice in many applications.

Among region-based methods, the level-set variational technique introduced by Chan and Vese (C-V) [15] has garnered widespread attention due to its simplicity and effectiveness, particularly in the segmentation of images into two homogeneous regions. Despite its strength in handling homogeneity, the C-V model struggles in the presence of noise or when an intensity inhomogeneity exists across regions. As a result, segmentation in such challenging environments becomes more difficult, as the model cannot fully adapt to variations in the image intensity, thus often leading to suboptimal results.

To overcome these limitations, numerous extensions and improvements have been proposed. The C-V model was expanded into a multi-phase model to handle more complex images with multiple regions [16]. However, while useful, this multi-phase approach still inherits the difficulties of noise sensitivity and intensity inhomogeneity. An important development in this area was the Local Binary Fitting (LBF) model proposed by Li et al. [19]. The LBF model enhances the C-V approach by incorporating a kernel function that better handles the intensity variations and noise, thus significantly improving the segmentation performance in more challenging scenarios.

Other advancements include the method by Ali et al. [20], which utilizes signed pressure generalized averages to segment inhomogeneous images with multiple objects. While effective, this approach has limitations, particularly when topological changes, such as contour merging or splitting, occur in the presence of noise. More recently, Ibrar et al. [21] developed a robust region-based model that integrates local similarity factors and local denoising constraints thus allowing it to handle noise and intensity variations. Despite its robustness, this method can encounter local minima due to the non-convexity of its functional, which increases the computational complexity.

Furthermore, the Adaptive Parameter Level Set Method (APLSM) proposed by Haiping et al. [22] offers an innovative approach to segmentation in highly inhomogeneous images. However, it faces challenges in scenarios where the images exhibit high levels of similarity among pixels, often getting stuck in local solutions due to a non-locality within the domain.

In this paper, we propose a novel convex region-based segmentation framework that addresses these challenges by introducing a comprehensive set of techniques for robust global segmentation (see Figure 1). Our model builds upon previous methods [19, 21] by incorporating a convolutional framework that averages the mean gray level entropy with image differences, local similarity factors, and spatial intensity differences. This results in a more precise level set function capable of capturing

intricate object boundaries, even in noisy and highly variable images. The combination of these elements significantly enhances the segmentation accuracy and reduces the computational complexity, thus offering an efficient and effective solution to the problem of image segmentation in complex scenarios.

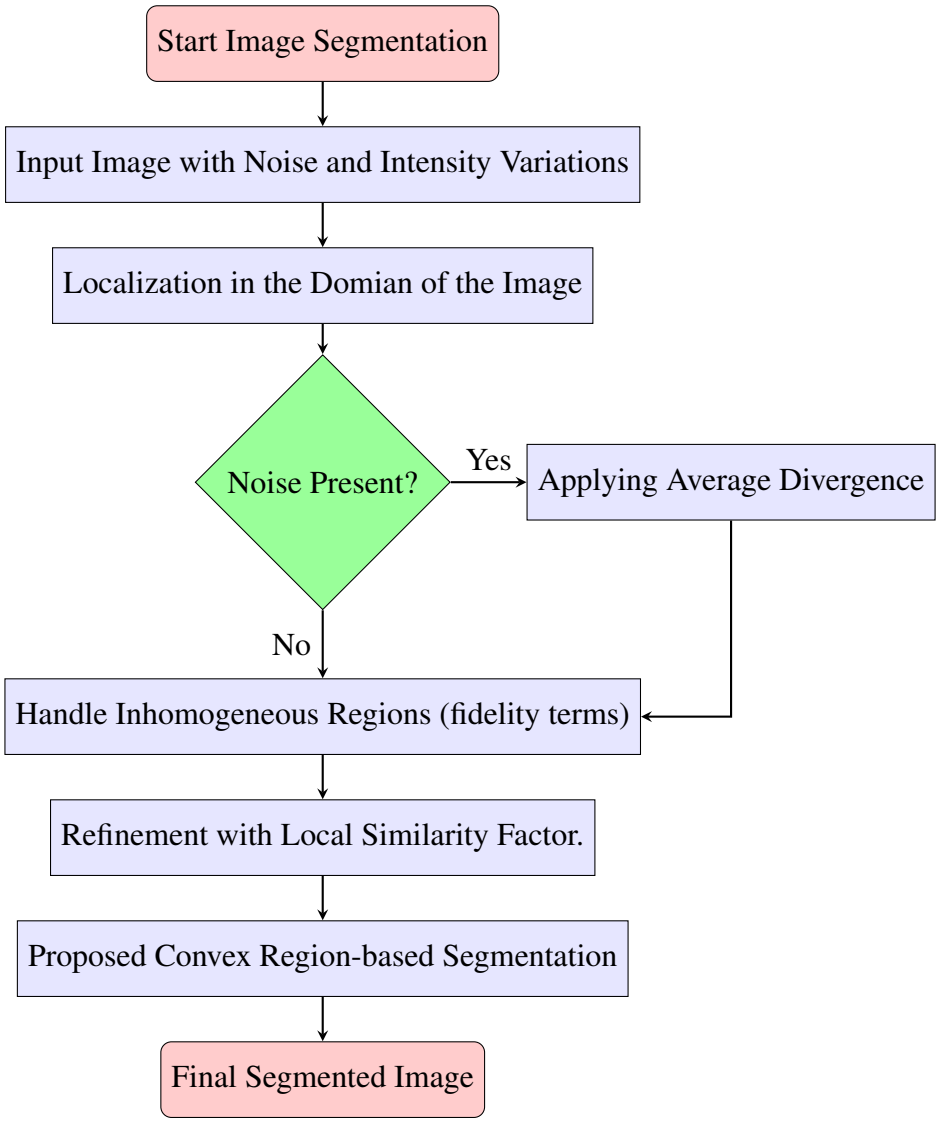

Figure 1. Flowchart for the segmentation process in proposed model.

To demonstrate the effectiveness of our model, we compared it with existing state-of-the-art methods on various datasets, including synthetic, outdoor, and medical images. Our experimental results show that our model provides superior accuracy and better segmentation outcomes compared to other approaches. The symbols and their corresponding meanings used throughout the text to facilitate understanding are summarized in Table 1.

Table 1. Symbols are used in the text to enable the reader to comprehend the discussion.

Symbol	Meaning	Symbol	Meaning
μ	parameter of length-term	φ	Level set
σ	scaled parameter	δ	Delta-function
g	Averaging filter	∇	Gradient
Ω	Bounded open-subset	ζ	energy functional parameter
z_0	Given image	ϵ	Diffusion term

This paper is structured as follows: Section 2 provides a review of related works in the field; Section 3 introduces the proposed segmentation model, including a detailed derivation of the Euler-Lagrange equation and its discretization; in Section 4, we present the experimental results using various datasets and compare the accuracy of our method with existing state-of-the-art approaches; and finally, Section 5 offers the concluding remarks on our work.

2. Previous work

2.1. Region based robust active contour technique

Let $z_0 : D \to \mathbb{R}$ be a given image, where D is the image domain; the energy functional of the region based robust active contour technique model [21] is defined as follows:

$$\begin{aligned} F(\varphi(\kappa_1)) &= \mu \int_{\kappa_2 \in Nbh_x} \delta_\epsilon(\varphi(\kappa_1))|\nabla\varphi(\kappa_1)|d\kappa \\ &+ (1-\zeta)\Big(\int_{\kappa_2 \in Nbh_x} \frac{\left|z_0(\kappa_1) - g_{c1}\right|^2}{d(\kappa_1,\kappa_2)} H_\epsilon(\varphi(\kappa_1)))d\kappa \\ &+ (1-\zeta)\Big(\int_{\kappa_2 \in Nbh_x} \frac{\left|z_0(\kappa_1) - g_{c2}\right|^2}{d(\kappa_1,\kappa_2)} (1 - H_\epsilon(\varphi(\kappa_1))))d\kappa \\ &+ \zeta \int_{\kappa_2 \in Nbh_x} \Big(\log z(\kappa_1) + \frac{z_0(\kappa_1)}{z(\kappa_1)} \Big) d\kappa. \end{aligned} \tag{2.1}$$

In this context, Nbh_x represents a local window that defines the neighborhood of pixels around a given pixel κ_1. The term $d(\kappa_1, \kappa_2)$ denotes the spatial Euclidean metric of any two pixels, κ_1 and κ_2. Additionally, g_{c1}, g_{c2} refer to the average intensities of the pixels inside and outside the contour, respectively.

The limitations of this method include the computational complexity, especially for large images, and the sensitivity to parameter tuning, which requires a careful adjustment for optimal performance. While the model handles high noise, it may still struggle with extremely noisy images or complex intensity inhomogeneity. Additionally, its performance may be limited for images with low contrast or weak edges. The local similarity factor improves the segmentation but may not perform well in cases where a global context is more important. Finally, the model risks overfitting, particularly when trained on specific datasets, and lacks consideration of the entropy concept, which could provide a further robustness in handling uncertainty and variations in image characteristics.

2.2. Bias correction based segmentation

The bias correction based segmentation (BC) model [23] processes an image by collecting localized information from regions with varying intensities (inhomogeneous areas). It leverages an energy-based approach, specifically an image-fitting energy function, to accurately capture the details within the image. Instead of processing each pixel independently, the model simultaneously computes the values of all pixels, thus ensuring a cohesive and detailed analysis of the entire image. This simultaneous calculation allows the model to efficiently handle noise and intensity variations, thus improving the segmentation accuracy in complex images. The mathematical framework of this model is given by the following:

$$E_L(x, y) = \left| Q(x, y) - \frac{1}{M} \sum_{i=1}^{M} Q(y_i, x_i) \right|^2, \tag{2.2}$$

where M represents the number of neighboring pixels considered for the local mean intensity computation.

2.2.1. Gradient term

The pixel-level gradient term assesses variations in the image gradients within a small neighborhood, helping to detect edges in the image. It is defined as follows:

$$E_{\text{grad}}(x, y) = |\nabla I(x, y)|^2. \tag{2.3}$$

2.2.2. Global intensity term

To account for the broader image context, the global intensity term captures the dissimilarity between the pixel intensity $I(x, y)$ and the global mean intensity. It is given by the following:

$$E_{\text{global}}(x, y) = \left| Q(x, y) - \frac{1}{M} \sum_{j=1}^{M} I(x_j, y_j) \right|^2. \tag{2.4}$$

2.2.3. Regularization term

A regularization term is incorporated to promote contour smoothness during evolution. It penalizes fluctuations in the level set function $\phi(x, y)$ as follows:

$$E_{\text{reg}}(x, y) = |\nabla \phi(x, y)|^2. \tag{2.5}$$

2.2.4. Hybrid energy function

The hybrid energy function combines both local and global information, with their contributions weighted by w_{local} and w_{global}, respectively:

$$E_{\text{hybrid}}(x, y) = w_{\text{local}} \cdot (E_L(x, y) + E_{\text{grad}}(x, y)) + w_{\text{global}} \cdot (E_{\text{global}}(x, y) + E_{\text{reg}}(x, y)). \tag{2.6}$$

The hybrid energy function combines both local and global intensity information, thereby facilitating a comprehensive analysis of the image that ensures accurate segmentation.

This model is vulnerable to robust noise, where significant noise in the image makes it difficult for the algorithm to distinguish between the actual object boundaries and noise artifacts. Since the model depends on the local intensity information, excessive noise can disrupt the accurate evolution of the active contour, leading to either premature or incorrect convergence, which ultimately affects the segmentation quality.

3. Proposed model

In this section, we propose a new approach to image segmentation that leverages an entropy-based technique combined with an averaging operator. Our method aims to effectively segment images, whether they contain noise or not, while preserving the detailed local information and fine features of the image. We benefit from the average local similarity factor, which is utilized in the local sense. In this way, our model will be able to tackle noisy and intensity inhomogeneity images. The proposed model can locally analyze the noise patterns in given image.

3.1. Introducing the average convolution with entropy mean gray level value

In an image analysis, pixels in a given image often have intensities similar to their neighboring pixels. Active contour models use local statistical information to segment the image, where each pixel's contribution is weighted by its distance from the center of a local window. To ensure that the local window size is appropriate, it should not exceed the size of the local region being examined. To address the limitations of traditional active contour methods, particularly their sensitivity to various types of noise, we propose incorporating the average convolution with entropy-based mean gray level values. This approach helps balance the intensity differences between neighboring pixels and the average intensity within the local interior and exterior regions. By using this method, we aim to improve the robustness of segmentation against different types and strengths of noise, which is a common shortcoming in existing region-based ACMs. In the average convolution with entropy mean gray level value, we used the average difference operator with a local similarity factor to build the region-based energy functional, which is defined pixel-by-pixel within the image $z_0(\kappa_1, \kappa_2)$. Let $C(\kappa_1, \kappa_2)$ denote the average gray-level value of neighboring pixels around the pixel (κ_1, κ_2) in the image $z_0(\kappa_1, \kappa_2)$, where $\kappa_1 = 1, 2, 3, \ldots, m$ and $\kappa_2 = 1, 2, 3, \ldots, n$. The local-region relative entropy of the pixel (κ_1, κ_2) is measured in a $m \times n$ neighborhood (Nbhd) as follows:

$$I(\kappa_1, \kappa_2) = \sum_{i,j=\frac{-m+1}{2}}^{\frac{m-1}{2}} z_0(\kappa_1, \kappa_2)(\kappa_1 + i, \kappa_2 + j) \times \frac{|log(z_0(\kappa_1, \kappa_2)(\kappa_1 + i, \kappa_2 + j))|}{C(\kappa_1, \kappa_2)}, \tag{3.1}$$

where $C(\kappa_1, \kappa_2)$ represents the average gray-level value of neighboring pixels around a particular pixel. This value is calculated as follows:

$$C(\kappa_1, \kappa_2) = \sum_{(i,j)=\frac{-m+1}{2}}^{\frac{m-1}{2}} z_0(\kappa_1, \kappa_2)(\kappa_1 + j, \kappa_2 + k).$$

Therefore, the average convolution with entropy mean gray level value function is given by the following:

$$ACE(x,c) = \int_{(y\in Nbh_x)\neq x} \frac{1}{M}(\left\|g * I(\kappa_1,\kappa_2) - I(\kappa_1,\kappa_2) - c\right\|^2)H_\epsilon(x)dx, \tag{3.2}$$

where Nbh_x is a local-window, defined as a neighborhood of pixels in the given area pixel κ_1, g denotes the averaging factor, and c represents the average intensity within the local region. $H_\epsilon(x)$ represents a regularized Heaviside function. The variable M denotes the number of adjacent pixels used to calculate the local mean intensity.

3.2. Functional of proposed model

For an image $z_0 : \Omega \to \mathrm{R}$, where Ω is the domain of z_0 , the functional of the proposed algorithm is followed by:

$$\begin{aligned} F_{(\varphi,c_1,c_2)} =& \zeta_1\Big(\int_{(\kappa_2\in Nbh_x)} \frac{1}{M}(\left|g * I(\kappa_1,\kappa_2) - I(\kappa_1,\kappa_2) - c_1\right|^2)H_\epsilon(\varphi(\kappa_1))d\kappa \\ &+ \int_{(\kappa_2\in Nbh_x)} \frac{1}{M}(\left|g * I(\kappa_1,\kappa_2) - I(\kappa_1,\kappa_2) - c_2\right|^2)(1 - H_\epsilon(\varphi(\kappa_1)))d\kappa\Big) \\ &+ \zeta_2\Big(\int_{(\kappa_2\in Nbh_x)} |I(\kappa_1,\kappa_2) - d_1|^2 H_\epsilon(\varphi(\kappa_1))d\kappa \\ &+ \int_{(\kappa_2\in Nbh_x)} |I(\kappa_1,\kappa_2) - d_2|^2(1 - H_\epsilon(\varphi(\kappa_1))d\kappa\Big) \\ &+ \mu\int_{(\kappa_2\in Nbh_x)} \delta_\epsilon(\varphi(\kappa_1))|\nabla\varphi(\kappa_1)|d\kappa. \end{aligned} \tag{3.3}$$

In this context, g is the averaging factor applied through convolution with the filtered image $I(\kappa_1,\kappa_2)$. The term c_1, d_1 represents the average intensities within the contour, while c_2, d_2 denotes the average intensities outside the contour.

$$\begin{cases} c_1 = \frac{\int_{(\kappa_2\in Nbh_x)\neq x} I(\kappa_1,\kappa_2)H_\epsilon(\varphi(\kappa_1))d\kappa}{\int_{(\kappa_2\in Nbh_x)\neq x} H_\epsilon(\varphi(\kappa_1))d\kappa}, \\ c_2 = \frac{\int_{(\kappa_2\in Nbh_x)\neq x} I(\kappa_1,\kappa_2)(1-H_\epsilon(\varphi(\kappa_1)))d\kappa}{\int_{(\kappa_2\in Nbh_x)\neq x}(1-H_\epsilon(\varphi(\kappa_1)))d\kappa}, \end{cases} \tag{3.4}$$

$$\begin{cases} d_1 = \frac{\int_{(\kappa_2\in Nbh_x)\neq x} I(\kappa_1,\kappa_2)(g-1)H_\epsilon(\varphi(\kappa_1))d\kappa}{\int_{(\kappa_2\in Nbh_x)\neq x} H_\epsilon(\varphi(\kappa_1))d\kappa}, \\ d_2 = \frac{\int_{(\kappa_2\in Nbh_x)\neq x} I(\kappa_1,\kappa_2)(g-1)(1-H_\epsilon(\varphi(\kappa_1)))d\kappa}{\int_{(\kappa_2\in Nbh_x)\neq x}(1-H_\epsilon(\varphi(\kappa_1)))d\kappa}. \end{cases} \tag{3.5}$$

By minimizing Eq (3.3), the following variational formulation can be obtained:

$$\begin{aligned} \frac{\partial\varphi}{\partial t} &= \delta_\epsilon(\varphi(\kappa_1))\Big[\mu\nabla\cdot\frac{\nabla\varphi(\kappa_1)}{|\nabla\varphi(\kappa_1)|} + \zeta_1\frac{\left(g * I(\kappa_1,\kappa_2) - I(\kappa_1,\kappa_2) - d_2\right)^2}{M} \\ &- \zeta_1\frac{\left(g * I(\kappa_1,\kappa_2) - I(\kappa_1,\kappa_2) - d_1\right)^2}{M} + \zeta_2\big((I(\kappa_1,\kappa_2) - c_1)^2 - (I(\kappa_1,\kappa_2) - c_2)^2\big)\Big]. \end{aligned}$$

This is denoted by the following:

$$\begin{aligned}\gamma_1 &= \frac{\left(g * I(\kappa_1,\kappa_2) - I(\kappa_1,\kappa_2) - d_2\right)^2}{M},\\ \gamma_2 &= \frac{\left(g * I(\kappa_1,\kappa_2) - I(\kappa_1,\kappa_2) - d_1\right)^2}{M},\\ \gamma_3 &= \left((I(\kappa_1,\kappa_2) - c_1)^2 - (I(\kappa_1,\kappa_2) - c_2)^2\right).\end{aligned} \tag{3.6}$$

The above equation can be written as follows:

$$\frac{\partial\varphi}{\partial t} = \delta_\epsilon(\varphi(\kappa_1))\Big[\mu\nabla\cdot\frac{\nabla\varphi(\kappa_1)}{|\nabla\varphi(\kappa_1)|} + \zeta_1\gamma_1 - \zeta_1\gamma_2 + \zeta_2\gamma_3\Big]. \tag{3.7}$$

3.3. Numerical scheme

The above parabolic equation can be solved by using the central-finite differences for discretization, which is given as follows:

$$\frac{\varphi_{i,j}^{n+1} - \varphi_{i,j}^{n}}{\Delta t} = \delta_\epsilon(\varphi_{i,j}^{n})\Big[\mu\kappa_\varphi + \zeta_1\gamma_1 - \zeta_1\gamma_2 + \zeta_2\gamma_3\Big],$$

or

$$\varphi_{i,j}^{n+1} = \varphi_{i,j}^{n} + \Delta t\delta_\epsilon(\varphi_{i,j}^{n})\Big[\mu\kappa_\varphi + \zeta_1\gamma_1 - \zeta_1\gamma_2 + \zeta_2\gamma_3\Big]. \tag{3.8}$$

With κ_φ, the curvature is calculated according to the given formula:

$$\kappa_\varphi = div(\frac{\nabla\varphi}{|\nabla\varphi|}) = \frac{\varphi_{xx}\varphi_y^2 - 2\varphi_{xy}\varphi_x\varphi_y + \varphi_{yy}\varphi_x^2}{(\varphi_x^2+\varphi_y^2)^{3/2}}, \tag{3.9}$$

where φ_x, φ_y, φ_{xx}, φ_{yy}, and φ_{xy} are computed as follows:

$$\begin{aligned}\varphi_x &= \frac{1}{2p}(\varphi_{i+1,j} - \varphi_{i-1,j}),\ \varphi_y = \frac{1}{2p}(\varphi_{i,j+1} - \varphi_{i,j-1}),\\ \varphi_{xx} &= \frac{1}{p^2}(\varphi_{i+1,j} + \varphi_{i-1,j} - 2\varphi_{i,j}),\ \varphi_{yy} = \frac{1}{p^2}(\varphi_{i,j+1} + \varphi_{i,j-1} - 2\varphi_{i,j}),\\ \varphi_{xy} &= \frac{1}{p^2}(\varphi_{i+1,j+1} - \varphi_{i-1,j+1} - \varphi_{i+1,j-1} + \varphi_{i-1,j-1}).\end{aligned} \tag{3.10}$$

Here, p refers to the grid size. The steps for the proposed method are outlined in Algorithm 1.

Algorithm 1. The proposed algorithm: $(\varphi^{n+1}(\kappa_1))) \leftarrow \left(\varphi^{(n)}, z_0, \zeta_1, \zeta_2, \zeta_3, \mu,\ \text{maxit,tol}\ \right)$.

1. Initialize the level-set function $\varphi(\kappa)$ with $\varphi^0(\kappa)$.
2. c_1, c_2 and d_1, d_2 are updated via (3.4) and (3.5).
3. Compute $\varphi^{n+1}(\kappa)$ using Eq (3.8).
4. Check weather the solution is stationary, $\left|\varphi_{i,j}^{n+1} - \varphi_{i,j}^{n}\right| \geq$ tol. If not, repeat step 2.

3.4. Convexity of proposed model

To check the convexity of the proposed model, we differentiate the energy functional twice using the following convexity theorem:

Theorem 3.1. *A Function is convex on interval I if and only if its second derivative f'' is non-negative for every x in I.*

To prove the energy functional is convex, we consider

$$\begin{aligned} F &= \frac{\left|I(\kappa_1,\kappa_2)(g-1)-c_1\right|^2}{M}H_\epsilon(\varphi(\kappa_1)) + \frac{\left|I(\kappa_1,\kappa_2)(g-1)-c_2\right|^2}{M}(1-H_\epsilon(\varphi(\kappa_1))) \\ &+ |I(\kappa_1,\kappa_2)-d_1|^2 H_\epsilon(\varphi(\kappa_1)) + |I(\kappa_1,\kappa_2)-d_2|^2(1-H_\epsilon(\varphi(\kappa_1)) + \delta_\epsilon(\varphi(\kappa_1))|\nabla\varphi(\kappa_1)|, \end{aligned}$$

such that $E = \int_\Omega F dxdy$. Suppose that $s_1 = (t_1, w_1), s_2 = (t_2, w_2)$; for any $t \in [0,1]$, we have the following:

$$\begin{aligned} ts_1 + (1-t)s_2 &= t(t_1,w_1) + (1-t)(t_2,w_2) \\ &= t(t_1-t_2) + t_2, t(w_1-w_2) + v2. \end{aligned} \tag{3.11}$$

Since $t_1, t_2 \in S$, $t_1 - t_2 \in S$ and $t \in [0,1]$; this implies that, $t(t_1-t_2)+t_2 \in S$ and $w_1 - w_2 \in S$. Therefore, $t(w_1-w_2)+w_2 \in S$, and hence $ts_1 + (1-t)s_2 \in \Omega$; thus, the domain Ω is convex. Now, to check the convexity of E, we partially differentiate F with respect to $I(\kappa_1,\kappa_2)$:

$$\begin{aligned} \frac{\partial F}{\partial I(\kappa_1,\kappa_2)} &= \frac{2\big(I(\kappa_1,\kappa_2)(g-1)-c_1\big)}{M}H_\epsilon(\varphi(\kappa_1))(g-1) \\ &+ \frac{2\big(I(\kappa_1,\kappa_2)(g-1)-c_2\big)}{M}(1-H_\epsilon(\varphi(\kappa_1)))(g-1) \\ &+ 2(I(\kappa_1,\kappa_2)-d_1)H_\epsilon(\varphi(\kappa_1)) + 2(I(\kappa_1,\kappa_2)-d_2)(1-H_\epsilon(\varphi(\kappa_1))). \end{aligned}$$

Again, differentiate with respect to $I(\kappa_1,\kappa_2)$:

$$\begin{aligned} \frac{\partial F^2}{\partial I_0^2} =& \frac{2H_\epsilon(\varphi(\kappa_1))(g-1)(g-1)}{M} + \frac{2(1-H_\epsilon(\varphi(\kappa_1)))(g-1)(g-1)}{M} \\ &+ 2H_\epsilon(\varphi(\kappa_1)) + 2(1-H_\epsilon(\varphi(\kappa_1)), \end{aligned} \tag{3.12}$$

$$\begin{aligned} \frac{\partial F^2}{\partial I_0^2} &= \frac{2H_\epsilon(\varphi(\kappa_1))(g-1)^2 + 2(1-H_\epsilon(\varphi(\kappa_1)))(g-1)^2}{M} \\ &+ 2H_\epsilon(\varphi(\kappa_1)) + 2(1-H_\epsilon(\varphi(\kappa_1)), \\ \frac{\partial F^2}{\partial I_0^2} &= \frac{2(g-1)^2\big(H_\epsilon(\varphi(\kappa_1)) + 1 - H_\epsilon(\varphi(\kappa_1))\big)}{M} + 2H_\epsilon(\varphi(\kappa_1)) + 2 - 2H_\epsilon(\varphi(\kappa_1)), \\ \frac{\partial F^2}{\partial I_0^2} &= \frac{2(g-1)^2}{M} + 2, \\ \frac{\partial F^2}{\partial I_0^2} &= \frac{2(g-1)^2}{M} + 2 \geq 0. \\ \frac{\partial F^2}{\partial I_0^2} &\geq 0. \end{aligned} \tag{3.13}$$

Hence proved. The energy functional is convex.

4. Experimental results

This section presents the experimental results for our proposed model, tested on both real and synthetic images to assess its performance. We compared our method with other approaches, specifically the APLSM model [22], BC model [23], and the method by Ibrar et al. [21], using images affected by noise and intensity inhomogeneity. To ensure a fair comparison, we used the parameters listed in Table 2, with a local window size of 5×5 and an image size of 110×110 pixels. The parameters for the proposed model were selected to optimize the performance across various noise conditions. The values of $\zeta_1 = 0.99$ and $\zeta_2 = 0.60$ were chosen to balance the noise suppression and boundary preservation, thus ensuring a robustness in images with high intensity variations. The smoothing parameter $\mu = 0.004$ was set to maintain the contour stability while adapting to noise, with smaller values enhancing the detail sensitivity. The parameter $\epsilon = 0.08$ was adjusted to prevent a numerical instability and to improve the convergence in noisy conditions. Unlike the BC model, the proposed approach does not heavily rely on the time step δt, as the entropy-based smoothing reduces a dependence on iterative updates. For Ibrar et al.'s model, the neighborhood size parameter $r = 10$ was selected to optimize the local region-based calculations for inhomogeneous regions. These parameters were empirically tested and adjusted based on the image characteristics, such as the noise type and intensity, thus ensuring the proposed model's adaptability and effectiveness. To validate the effectiveness of the proposed model, extensive statistical experiments were conducted. Statistical metrics, including Accuracy, Precision, Recall, F1-Score, Intersection over Union (IoU), Dice Coefficient, Matthews Correlation Coefficient (MCC), Peak Signal-to-Noise Ratio (PSNR), and Structural Similarity Index Measure (SSIM), were utilized to quantify the enhancements. The results indicated that the proposed model achieved an average improvement over the baseline models in high-noise scenarios.

Table 2. Parameters utilized for BC, Ibrar et al., and the proposed model.

BC	Parameters	Ibrar et al.	parameters	Proposed model	Parameters
ζ	0.4	ζ	0.98	ζ_1	0.99
				ζ_2	0.60
μ	4	μ	0.001	μ	0.004
ϵ	0.5	ϵ	0.04	ϵ	0.08
δ t	0.2	r	10		

All experiments were conducted on a 1.00 GHz Intel Core m PC with 4GB of RAM running Windows 10. The algorithm was implemented in Matlab 7.9.0. For research purposes, the code for our method can be provided upon request via email.

First, the proposed model used the average convolution to entropy mean gray level value with image difference technique to smooth the image and displayed the noise clear in the given image. Figures 2 and 3 are the adequately explained machine results of propose model. We further evaluate our proposed model by comparing its segmentation accuracy with that of other models, as illustrated in Figure 4. In this figure, the segmented images are shown row by row from left to right. The second and third columns feature the BC model and the method by Ibrar et al., respectively. These models effectively detect the object boundaries; however, in the first row, which shows different layers of the sky background, these methods struggle with segmentation, due to non-convexity and high intensity

inhomogeneity and noise, thus failing to accurately segment the image. In the second row, both the BC and Ibrar et al. models encounter difficulties and get stuck to segment the image, thus impacting their performance. The proposed model segments Figure 4 locally by utilizing the average convolution to entropy mean gray level value with image difference technique.

We assessed the performance of the proposed method under various noise conditions and compared its effectiveness with other models, including the APLSM model, the BC model, and the method by Ibrar et al. For the evaluation, we used specific parameters for the proposed model, as detailed $\zeta_1 = 0.99$, $\zeta_2 = 0.6$. To make a precise comparison between the proposed model and other models, we introduced artificial speckle noise with parameters δ=(0.03, 0.03) to the images using the imnoise function in Matlab. Additionally, we used the same initial contour for all models in the comparison. We utilize advantages from the relative entropy in the proposed model shown in Figure 5, where the proposed model has best segmentation accuracy as compared to the APLSM [22].

In addition, our proposed model is convex, which shows better results as compare to the APLSM model and the ibrar et al. [21] model in Figures 4 and 5, respectively. Additionally, Figure 6 demonstrates that using different initial contours yields the same segmentation results. This consistency indicates that the energy functional we designed is convex. Table 3 provides a comprehensive comparison of the segmentation performance metrics across different models, including Accuracy, Precision, Recall, F1-Score, IoU, Dice Coefficient, and MCC. The proposed model consistently outperformed APLSM, Ibrar et al., and the BC model across all metrics. Specifically, the proposed model achieved the highest Accuracy (94.0%), Precision (94.5%), Recall (92.8%), and F1-Score (93.6%), thus demonstrating its superior classification capabilities. Additionally, it recorded an IoU of 89.4% and a Dice Coefficient of 94.3%, which indicate excellent segmentation overlaps and similarities with the ground truth data. The MCC of 90.8% further highlights the proposed model's robustness and reliability, especially in handling imbalanced datasets. These results validate the effectiveness of the proposed model in achieving accurate and reliable segmentation compared to existing methods, as displayed in Figure 7.

The proposed method not only provides a high accuracy, but also operates faster than existing methods. Table 4 compares the speed of the competing models with the proposed model, thus highlighting the efficiency of our approach in terms of time and the number of iterations required.

Table 5 highlights the performance of the proposed model compared to APLSM, BC, and Ibrar et al.'s methods under Gaussian noise conditions. The proposed model consistently outperformed other approaches, thereby achieving the highest PSNR and SSIM values.

Under Gaussian noise with $\sigma = 0.1$, the proposed model achieved a PSNR of 30.91 dB and an SSIM of 0.910, which corresponds to a 21.5% improvement in PSNR and a 5.0% increase in SSIM compared to Ibrar et al.'s method. Similarly, compared to the BC model, the proposed model exhibited a 9.0% improvement in PSNR and a 5.0% increase in SSIM. These results demonstrate the robustness of the proposed model in effectively handling Gaussian noise.

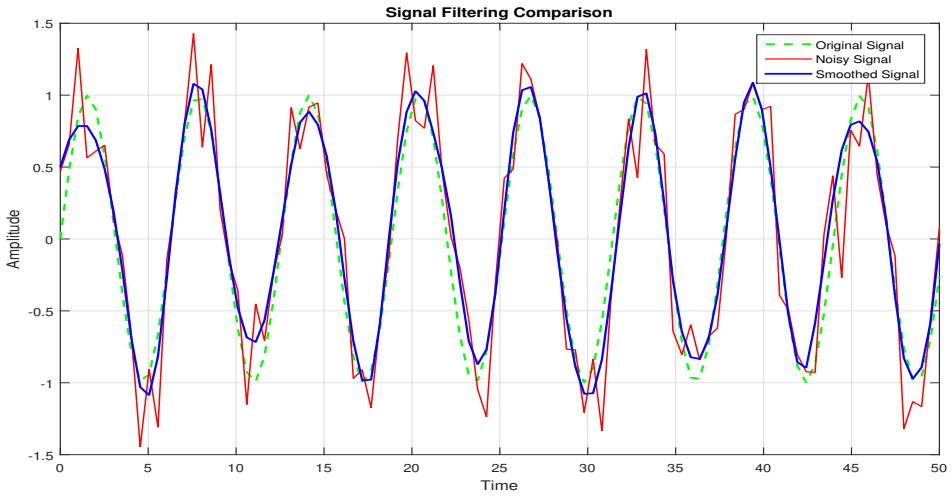

Figure 2. Image smoothing process using average convolution in the propose model.

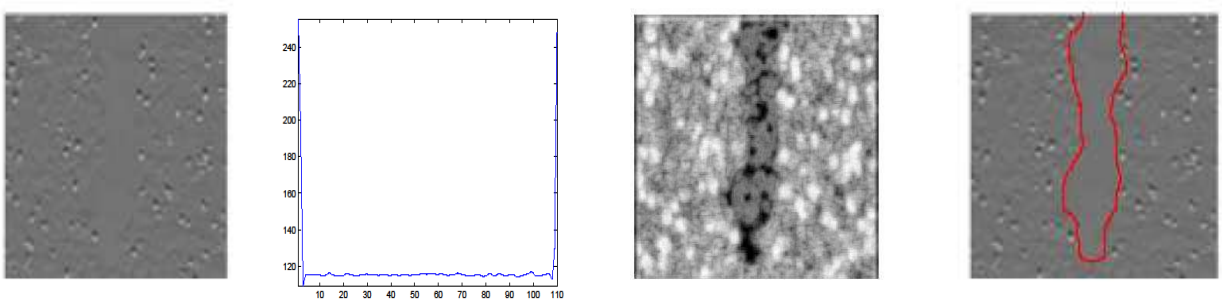

Figure 3. Image having same pixel values applying entropy technique and segmentation result of proposed model.

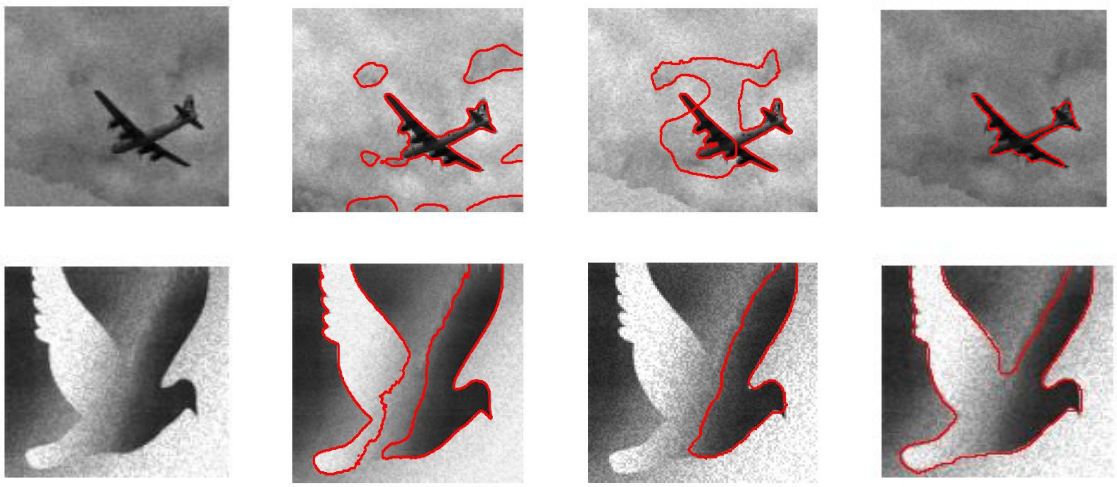

Figure 4. Segmentation results of BC, Ibrar et al. and the proposed model.

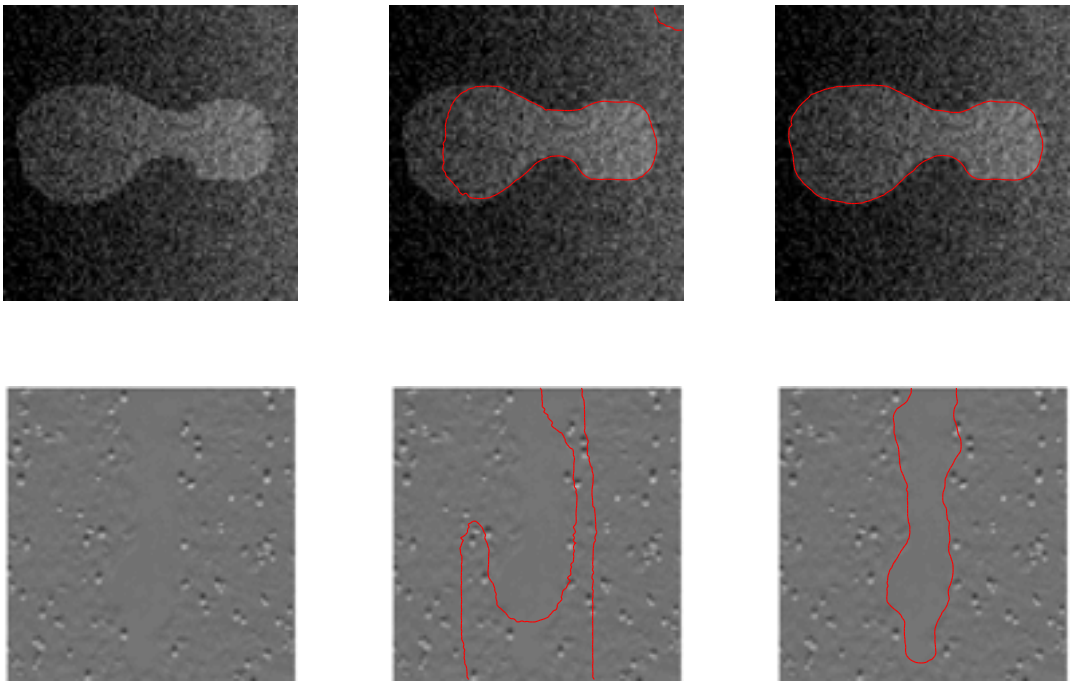

Figure 5. The given image, and results of APLSM and the new proposed model in second and third coloumn respectively.

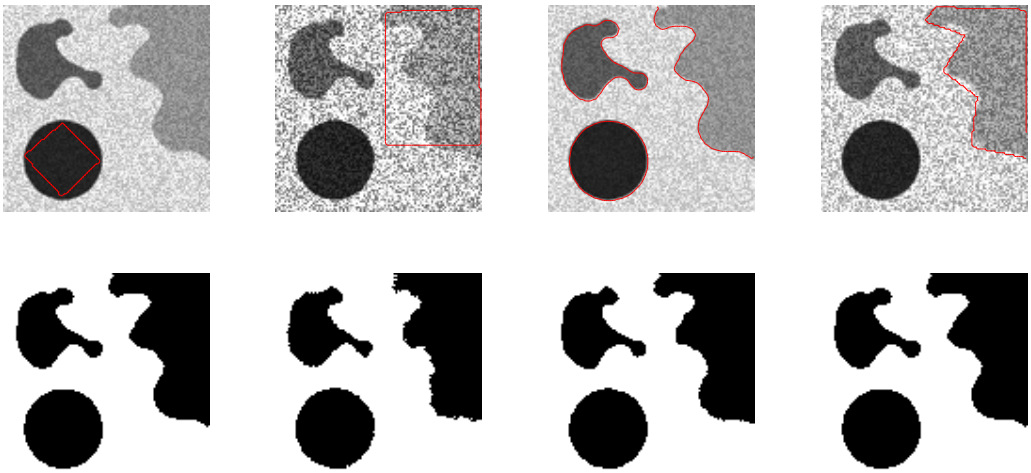

Figure 6. Identical results obtained from various initial contours indicate the convexity of the designed functional.

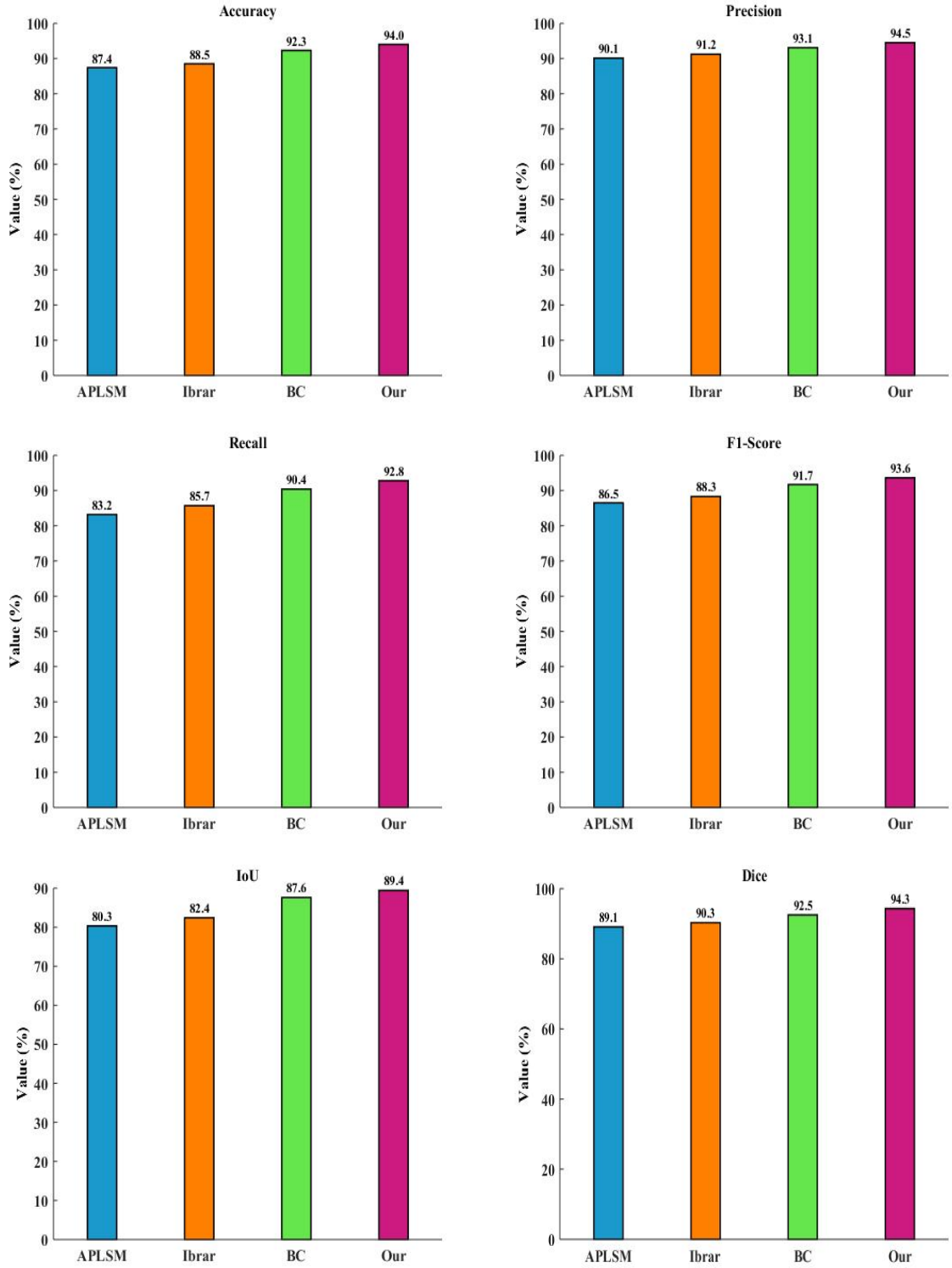

Figure 7. Comprehensive evaluation metrics for segmentation performance of the competing models and propose model, using Table 3.

Table 3. Comprehensive evaluation metrics for segmentation performance.

Model	Accuracy	Precision	Recall	F1-Score	IoU	Dice	MCC
APLSM	87.4	90.1	83.2	86.5	80.3	89.1	78.5
Ibrar	88.5	91.2	85.7	88.3	82.4	90.3	80.2
BC	92.3	93.1	90.4	91.7	87.6	92.5	85.7
Our	94.0	94.5	92.8	93.6	89.4	94.3	90.8

Table 4. Proficiency comparison of the APLSM [22], BC [23], Ibrar et al. [21], and proposed model.

APLSM		Ibrar et al. model		BC model		Proposed model	
Iteration	CPU	Iteration	CPU	Iteration	CPU	Iteration	CPU
		150	38.91	100	28.91	60	20.45
		150	39.75	100	33.75	60	22.07
200	62.31					80	26.07
300	74.54					60	22.42

Table 5. Performance comparison of PSNR and SSIM for various models.

Model	Noise type	PSNR (dB)	SSIM
APLSM	Gaussian ($\sigma = 0.1$)	25.43	0.812
Ibrar et al.	Gaussian ($\sigma = 0.1$)	27.21	0.846
BC	Gaussian ($\sigma = 0.1$)	28.54	0.867
Proposed model	Gaussian ($\sigma = 0.1$)	**30.91**	**0.910**

5. Conclusions

In image segmentation, our proposed model was shown to effectively handle images with Speckle noise and intensity inhomogeneity during iterative processing, thereby outperforming many other variational segmentation models that struggle with severe noise. Additionally, the high accuracy of our algorithm resulted in an improved computational efficiency. This model has potential applications in real-world scenarios such as medical image segmentation, including tumor detection and identifying affected areas in cancer diagnoses. We are happy to provide the code for research purposes upon request via email.

However, the proposed model has some limitations: (a) It encounters difficulties with multi-phase segmentation; and (b) its reliance on entropy can overlook similar pixels, thus leading to over-segmentation, where an image is divided into too many regions. This occurs because the method might detect small changes in entropy as significant boundaries, thus leading to excessive segmentation. Addressing these limitations could offer valuable avenues for future research in computational mathematics and image processing.

Author contributions

Both authors contributed significantly to the research. Ming Shi developed the novel segmentation approach, refining the mathematical framework and integrating entropy-based methods. His work on the local similarity factor (LSF) and local region relative entropy (L-RE) was key to enhancing the robustness of the energy functional. Ibrar Hussain conducted the formal analysis and validated the model through experiments under varying noise levels. Both authors collaborated on drafting, reviewing, and editing the manuscript. Additionally, Ming Shi supervised the project and secured funding, while Ibrar Hussain assisted with administrative tasks. Both authors read and approved the final manuscript.

Use of Generative-AI tools declaration

The authors declare that they have not used Artificial Intelligence (AI) tools in the creation of this article.

Conflict of interest

The authors declare that there is no conflict of interest regarding the publication of this paper.

References

1. H. Ibrar, J. Muhammad, Efficient convex region-based segmentation for noising and inhomogeneous patterns, *Inverse Probl. Imag.*, **17** (2023), 708–725. https://doi.org/10.3934/ipi.2022074
2. R. M. Abdelazeem, D. Youssef, J. El-Azab, S. Hassab-Elnaby, M. Agour, Three-dimensional visualization of brain tumor progression based accurate segmentation via comparative holographic projection, *PloS One*, **15** (2020), e0236835. https://doi.org/10.1371/journal.pone.0236835
3. I. Hussain, R. Ali, Robust leaf disease detection using complex fuzzy sets and HSV-based color segmentation techniques, *Acadlore Trans. Mach. Learn.*, **3** (2024), 183–192. https://doi.org/10.56578/ataiml030305
4. L. C. Chen, G. Papandreou, I. Kokkinos, K. Murphy, A. L. Yuille, DeepLab: Semantic image segmentation with deep convolutional nets, atrous convolution, and fully connected CRFs, *IEEE Trans. Pattern Anal. Mach. Int.*, **40** (2018), 834–848. https://doi.org/10.1109/TPAMI.2017.2699184
5. E. Calli, E. Sogancioglu, B. van Ginneken, K. G. van Leeuwen, K. Murphy, Deep learning for chest X-ray analysis: a survey, *Med. Image Anal.*, **72** (2021), 102125. https://doi.org/10.1016/j.media.2021.102125
6. I. Hussain, J. Muhammad, R. Ali, Enhanced global image segmentation: addressing pixel inhomogeneity and noise with average convolution and entropy-based local factor, *Int. J. Knowl. Innovation Stud.*, **1** (2023), 116–126. https://doi.org/10.56578/ijkis010204

7. M. S. Khan, A region-based fuzzy logic approach for enhancing road image visibility in foggy conditions, *Mechatron. Intell. Trans. Syst.*, **3** (2024), 212–222. https://doi.org/10.56578/mits030402

8. Ç. Kaymak, A. Uçar, A brief survey and an application of semantic image segmentation for autonomous driving, In: V. Balas, S. Roy, D. Sharma, P. Samui, *Handbook of deep learning applications*, Smart Innovation, Systems and Technologies, Springer, **136** (2019), 161–200. https://doi.org/10.1007/978-3-030-11479-4_9

9. B. Peng, L. Zhang, J. Yang, Iterated graph cuts for image segmentation, In: H. Zha, R. Taniguchi, S. Maybank, *Computer vision–ACCV 2009*, Lecture Notes in Computer Science, Springer, **5995** (2009), 677–686. https://doi.org/10.1007/978-3-642-12304-7_64

10. H. Lyu, H. Fu, X. Hu, L. Liu, Esnet: edge-based segmentation network for real-time semantic segmentation in traffic scenes, *2019 IEEE International Conference on Image Processing (ICIP)*, (2019), 1855–1859. https://doi.org/10.1109/ICIP.2019.8803132

11. W. Zhou, X. Du, S. Wang, Techniques for image segmentation based on edge detection, *IEEE International Conference on Computer Science, Electronic Information Engineering and Intelligent Control Technology (CEI)*, 2021, 400–403. https://doi.org/10.1109/CEI52496.2021.9574569

12. I. Hussain, An adaptive multi-stage fuzzy logic framework for accurate detection and structural analysis of road cracks, *Mechatron. Intell Transp. Syst.*, **3** (2024), 190–202. https://doi.org/10.56578/mits030305

13. D. Gupta, R. S. Anand, A hybrid edge-based segmentation approach for ultrasound medical images, *Biomed. Signal Proces. Control*, **31** (2017), 116–126. https://doi.org/10.1016/j.bspc.2016.06.012

14. S. Niu, Q. Chen, L. de Sisternes, Z. Ji, Z. Zhou, D. L. Rubin, Robust noise region-based active contour model via local similarity factor for image segmentation, *Pattern Recogn.*, **61** (2017), 104–119. https://doi.org/10.1016/j.patcog.2016.07.022

15. T. F. Chan, L. A. Vese, Active contours without edges, *IEEE Trans. Image Process.*, **10** (2001), 266–277. https://doi.org/10.1109/83.902291

16. L. A. Vese, T. F. Chan, A multiphase level set framework for image segmentation using the Mumford and Shah model, *Int. J. Comput. Vision*, **50** (2002), 271–293. https://doi.org/10.1023/A:1020874308076

17. A. Tsai, A. Yezzi, A. S. Willsky, Curve evolution implementation of the Mumford-Shah functional for image segmentation, denoising, interpolation, and magnification, *IEEE Trans. Image Process.*, **10** (2001), 1169–1186. https://doi.org/10.1109/83.935033

18. R. Ronfard, Region-based strategies for active contour models, *Int. J. Comput. Vision*, **13** (1994), 229–251. https://doi.org/10.1007/BF01427153

19. C. Li, C. Y. Kao, J. C. Gore, Z. Ding, Implicit active contours driven by local binary fitting energy, *IEEE Conference on Computer Vision and Pattern Recognition*, (2007), 1–7. https://doi.org/10.1109/CVPR.2007.383014

20. H. Ali, L. Rada, N. Badshah, Image segmentation for intensity inhomogeniety in presence of high noise, *IEEE Trans. Image Process.*, **8** (2018), 3729–3738. https://doi.org/10.1109/TIP.2018.2825101

21. H. Ibrar, H. Ali, M. S. Khan, S. Niu, L. Rada, Robust region-based active contour models via local statistical similarity and local similarity factor for intensity inhomogeneity and high noise image segmentation, *Inverse Probl. Imag.*, **16** (2022), 1113–1136. https://doi.org/10.3934/ipi.2022014

22. H. Yu, K. Ma, X. Lin, P. Sun, High-precision inhomogeneous image segmentation based on adaptive parameter level set method, *J. Adv. Mech. Des. Syst. Manuf.*, **18** (2024), 1–12. https://doi.org/10.1299/jamdsm.2024jamdsm0027

23. H. Zia, S. Soomro, K. N. Choi, Image segmentation using bias correction active contours, *IEEE Access*, **12** (2024), 60641–60655. https://doi.org/10.1109/ACCESS.2024.3391052

AIMS Press